Controlled interference of laser-induced shock waves in microdroplet jetting

R. A. Meijer,[1,*] G. Lajoinie,[2] B. Liu,[1] S. Witte,[1,3,†] and O. O. Versolato[1,3,‡]

[1]*Advanced Research Center for Nanolithography (ARCNL), Science Park 106, 1098 XG Amsterdam, The Netherlands*
[2]*Physics of Fluids Group, MESA+ Institute for Nanotechnology and Technical Medical (TechMed) Center, University of Twente, P.O. Box 217, 7500 AE Enschede, The Netherlands*
[3]*Department of Physics and Astronomy, and LaserLaB, Vrije Universiteit Amsterdam, De Boelelaan 1100, 1081 HV Amsterdam, The Netherlands*

(Received 17 December 2025; accepted 9 April 2026; published 12 June 2026)

We report the formation of high-velocity microjets driven by the interference of two laser-induced shock waves in a tin microdroplet. A first 0.4-ns laser pulse launches a shock wave into the droplet (diameter $D_0 = 40$, 50, and 60 μm). Due to the droplet's spherical geometry, the shock converges and diverges as it traverses the droplet center and reaches the back surface. Upon reflection from the free back surface, the shock reverses polarity, producing an intense, focused tensile wave. This wave nucleates an ~ 1 μm cavitation bubble, trapping itself on the front side of the droplet, between the bubble and the droplet's free laser-facing surface. Impact of a second, delayed, identical laser pulse introduces a second shock wave and leads to the formation of a microjet. Scanning the delay of this second pulse reveals a complex pattern of constructive and destructive interferences of the two shocks through the observed change in jet velocity, with velocities reaching 110 m/s. This laser-droplet system presents a unique case for the study of acoustics and cavitation at the microscale.

DOI: 10.1103/8ltx-t2xs

I. INTRODUCTION

The deposition of a substantial amount of energy into a confined liquid sample [1–4] initiates a plethora of rich physical processes, including shock-wave propagation and nucleation of cavitation bubbles, whose interaction and ensuing dynamics often lead to jetting [5–7] and fragmentation [8–11] of the liquid body. These strongly entwined phenomena are studied within the context of applications such as erosion in various liquid-mechanical systems [12–15], biomedical therapy, e.g., sonoporation [16,17] and needle-free injection [18–20], and tin-droplet-based EUV sources [21–27].

In this work, we present the first observation of fast jets generated by the interference of two subsequent laser-induced shock waves in a droplet. The pressure impulse generated by the impact of the first pulse excites a shock wave that propagates inside the droplet. Due to the spherical geometry, the shock focuses toward the center of the droplet, reflects off the backside of the droplet (reversing polarity) to focus again and induce cavitation through tensile breakup [26]. A second shock wave is generated by impact of a second, identical laser pulse that, through its interaction with both the vapor cavitation bubble and the first shock wave, leads to the formation of a microjet aligned with the laser-propagation direction with velocities up to 110 m/s. These shocks, generated via laser ablation, can have trailing negative peaks, contributing to instances of positive and destructive interference [26].

II. EXPERIMENTAL SETUP

A stream of liquid tin microdroplets is generated by flowing liquid tin (260 °C) through a specially designed nozzle vertically mounted in a vacuum chamber ($\simeq 10^{-7}$ mbar). A piezo element mounted on the nozzle allows for a controlled breakup of the stream at a chosen frequency (kilohertz range) into equal-sized droplets. At constant tin flow, we produce droplets of diameter $D_0 = 40$, 50, and 60 μm by varying the frequency of the modulation applied to the piezo element. Laser and acquisition systems are triggered by a pulse of light scattered by a droplet as it passes a laser sheet positioned slightly above the center of the vacuum vessel, i.e., the laser-droplet interaction point. The phenomena are observed stroboscopically at a real time of 10 Hz, using a trigger holdoff on the kilohertz-range signal generated by the droplet train crossing the laser sheet. More detailed descriptions of the setup can be found in Refs. [28,29].

Two temporally Gaussian-shaped laser pulses with a full width at half maximum (FWHM) duration of 0.4 ns, wavelength $\lambda = 1064$ nm, are incident on the droplet (cf. Ref. [27]) as illustrated in Fig. 1(a). Pulse-pair generation is automated using the arbitrary pulse-shaping capability of the laser system [30]. Combined with a feedback algorithm, it allows for a

*Present address: ASML, 17075 Thornmint Court, San Diego, California 92127, USA.

†Present address: Imaging Physics, Faculty of Applied Sciences, Delft University of Technology, Lorentzweg 1, 2628 CJ Delft, The Netherlands.

‡Contact author: versolato@arcnl.nl

Published by the American Physical Society under the terms of the Creative Commons Attribution 4.0 International license. Further distribution of this work must maintain attribution to the author(s) and the published article's title, journal citation, and DOI.

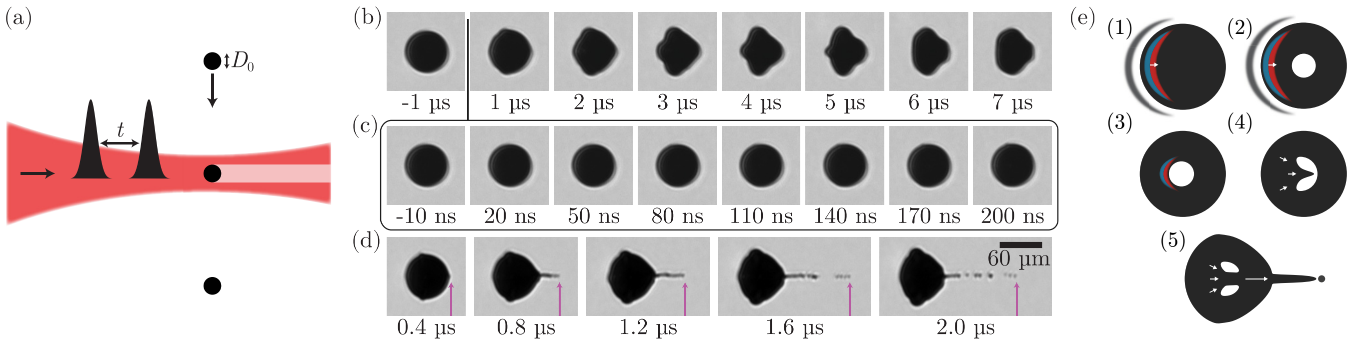

FIG. 1. (a) Illustration of the experiment. A tin droplet with a diameter D_0 is impacted by a pulse pair with a time delay between the two pulses t. The laser beam is focused at the position of the droplet with a Gaussian spatial profile. The two identical laser pulses have a Gaussian temporal profile. (b) Shadowgraphy series of a $D_0 = 60\,\mu$m tin droplet after being impacted by a single pulse only (equal to the first pulse of the pulse pair). Panel (c) provides an enlarged view on early times. (d) Example shadowgraphy series of double-pulse-induced jet formation for a $D_0 = 60\,\mu$m tin droplet after impact of a pulse pair with pulse spacing $t = 47.4$ ns. The arrow in each panel indicates the position of the jet tip or its furthest fragment. The time between (first) laser-pulse impact and the shadowgraphy recording is indicated below each image panel. Scale bar is common for all panels. (e) Illustration of the proposed jetting mechanism (cavitation bubble and jet not to scale).

convenient, accurate, and fully electronic tuning of the pulse amplitudes and spacing. The spacing between the two pulses t is scanned up to 200 ns with a minimum step size of 0.4 ns. The laser beam, with a circular polarization, is focused to a Gaussian spot of approximately 90 µm (FWHM) at the position of the droplet. For most of the study, the energies of the two pulses in the pulse pairs are kept identical, with the laser energy adjusted per droplet size such that the single-pulse energy per droplet volume E/R_0^3 is kept constant [26] at a value of 1.3×10^{-6} mJ/µm^3, unless otherwise indicated. This particular value is chosen to be, just, high enough to produce a small bubble while minimizing detrimental impact on acoustics or visible cavitation-driven expansion of the droplet resulting from even higher energies [25]. The single-pulse energy value is consistent with the $2(1) \times 10^{-6}$ mJ/µm^3 cavitation threshold obtained in previous work [29], extrapolating from single-pulse cavitation visible through the expansion of the droplet exterior. We note that femtosecond- or picosecond-duration pulses produce cavitation $\sim 2.5\times$ more efficiently [29] and would already produce violent cavitation tied to a visible expansion for the pulse energies used in this work. We also note that another order-of-magnitude increase in pulse energy is required to induce spallation on the backside of the droplet [23,25,26,31].

The droplet is backlit using an incoherent laser pulse with $\lambda \approx 560$ nm and the shadow created by the droplet is imaged on a camera using a long-distance microscope (Infinity K2 DistaMax CF-3, NA = 0.24). The spatial and (stroboscopic) temporal resolutions of this *shadowgraphy* setup positioned perpendicularly to the laser-propagation axis are approximately 3 µm and 5 ns, respectively. A recording of the droplet deformation is obtained by recording subsequent laser-droplet-impact events while gradually scanning the delay between the backlighting laser pulse and the pulse pair. From the shadowgraphy recordings, we obtain the position of the tip of the jet (or of the furthest fragment originating from the jet) over time by a simple thresholding step. From this trajectory, we determine a jet velocity $v_{\rm jet}$ with a linear fit.

III. INTERFERENCE JETTING

Figures 1(b) and 1(c) show, respectively, early- and late-time shadowgraphy recordings of a 60-µm-diameter droplet impacted by only one pulse. The droplet impacted by a single pulse shows minimal deformation within the first 200 ns and typical shape oscillations at later times. In the current experiment, no jet is observed without the impact of a second pulse. Single-pulse impact also leads to a slight forward propulsion of the droplet, with a velocity of approximately 3–6 m/s depending on droplet size [28,32]. Crucially, for the initial 200 ns, no measurable change in the droplet shape is observed with our threshold-based analysis. Moreover, photodiode measurements of reflected light from the droplet (as in Ref. [33]) show identical reflection amplitudes (within 10% after 20 ns) for both the first and second pulse. We thus conclude that the second pulse impacts an essentially undeformed, identical target.

Figure 1(d) shows a droplet impacted by two pulses with a pulse spacing $t = 47.4$ ns. Under these specific conditions, a jet emerges from the droplet on a 1-µs timescale. Note that any incompressible flow contributions to jetting, for example, from capillary waves, would occur on a much longer capillary timescale $\tau_c = \sqrt{\rho R_0^3/\sigma}$, with surface tension $\sigma = 0.544$ N/m and density $\rho = 7000$ kg/m^3, on the order of 10 µs, emphasizing that the here observed jetting is of a distinctly different origin. The vertical arrows in Fig. 1(d) give an indication of the jet-tip position, or the furthest fragment after breakup, used to determine $v_{\rm jet}$.

The jetting mechanism we hypothesize is illustrated in Fig. 1(e) and previously postulated by Hudgins *et al.* [34]. The second shock impacts the cavitation bubble's left side (panel 3), initiating a hydrodynamic focusing and formation of the jet (panel 4), which traverses the bubble and punctures the right side of the droplet (panel 5). We note that pulse-pair-induced jetting by tin microdroplets has been previously observed for considerably higher pulse energies [24,27] and for pulse trains [34]. In these cases, a jet is formed while the main droplet body expands into a single-, or double-shell-like structure.

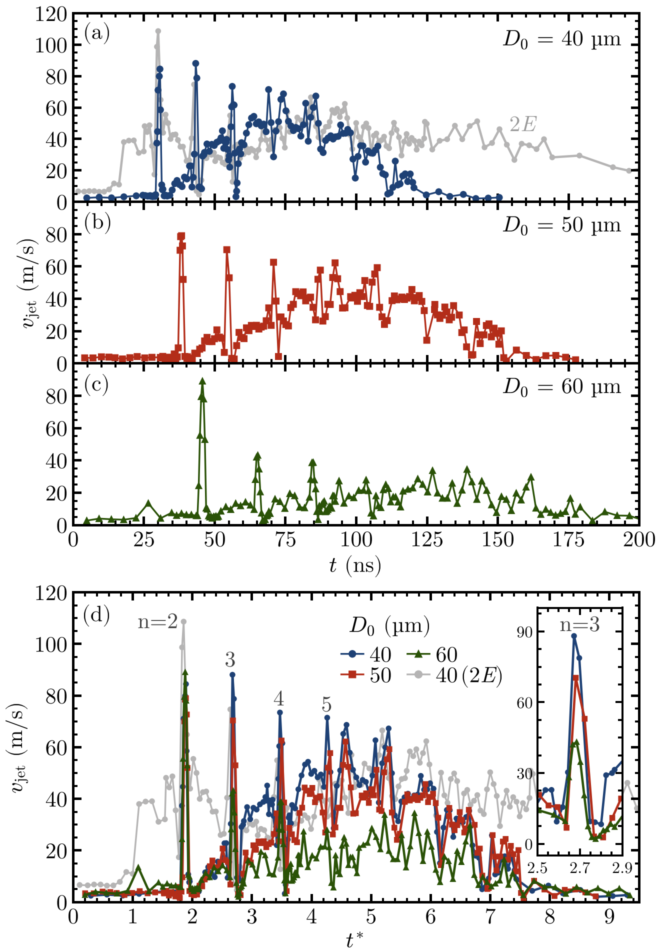

FIG. 2. (a)–(c) Jet velocity v_{jet} as a function of pulse spacing t for the three studied droplet diameters D_0 of 40, 50, and 60 µm. Panel (a) also contains a measurement, marked with $2E$, for which the laser-pulse energy was twofold that of the nominal value. (d) Jet velocity v_{jet} as a function of nondimensional round-trip time $t^* = tc/D_0$. The inset provides an enlarged view of the $n = 3$ peaks for the nominal-energy cases.

The jetting we observe here is thought to be similar to the jetting observed from a meniscus impacted by a shock [35,36] or similarly, the jetting mechanism studied within the context of shaped charges [37,38]. Interaction of bubbles in a bulk with a passing shock wave [16,39] also leads to an analogous type of jetting. An example more comparable to the jetting presented in this work is the observed jetting of bubbles close to a free surface after shock impact [5]. Several other related studies have focused on bubbles inside droplets [1,4], in some cases interacting with an external planar shock [40–42], which also results in similar observations of jetting. Interaction between shock waves and laser-generation bubbles has been studied previously also in Ref. [43]. The case presented here is unique in the nonplanar, but (spherically) converging shape of the shock-wave incident on a transient cavitation bubble located near the center of the droplet.

Figures 2(a)–2(c) show the obtained jet velocity v_{jet} as a function of pulse spacing t for the three different droplet sizes. All three curves show a baseline velocity v_{jet} that initially increases and then decreases. We hypothesize that the delay range of the background velocity corresponds to the lifetime of the cavitation bubble (see below). This shape is superimposed with distinct peaks and dips at early times, and an increasingly irregular structure at later times. By introducing a nondimensional acoustic propagation time $t^* = tc/D_0$, with $c = 2470\,\mathrm{m/s}$, the speed of sound in liquid tin at 260 °C [44], we obtain a near perfect overlap of the observed structure, indicating their acoustic origin [see Fig. 2(d)]. Note that the late-time, seemingly irregular structure is also reproduced between different droplet sizes, specifically for the 40 and 50 µm cases. These features can thus be assumed to have the same acoustic origins as the peaks, arising from more complex pressure fields that have developed inside the droplet at late times. The peaks and dips in the data are due to constructive and destructive interference of the two shock waves and its following effect on jet formation. In Fig. 2(d), we label the first four distinct peaks according to their order of appearance n, starting from $n = 2$ given the first peak's proximity to $t^* = 2$. Note that beyond $n = 5$, the structure becomes more complex and presents rich dynamics. No distinct features belonging to the same series can be identified beyond that point. Figure 2(a) also shows a measurement where a twofold higher laser energy $2E$ was used, generating a nearly unstructured background. The interferences, which remain visible, still overlap on the nondimensional timescale [cf. Fig. 2(d)]. The relation between a zero in the jet velocity and the degree of destructive interference is nontrivial, also given the complexities of shock-wave dynamics [45]. It may well be that the jet velocity drops to zero because the pressure was reduced below a threshold for jet formation. In this case, the interference would be fully destructive with respect to the resulting jet velocity, while being but partially destructive in pressure.

IV. ACOUSTICS, TRAPPING, AND INTERFERENCE

To explain the observed phenomena, we propose a model that is schematically depicted in Fig. 3. A first pressure wave is generated by the first laser pulse and traverses the drop. In the first passing of the center, the weaker rarefaction wave trailing the much larger positive pressure wave (cf. Ref. [26]) has insufficient amplitude to induce cavitation. Under these conditions, the reflection will also not lead to spallation (cf. Refs. [25,26]) (note that, in this description, n also corresponds to the number of reflections experienced by the first pulse on the external interface on the droplet). The reflection of the pressure wave at the free surface on the right-hand-side droplet reverses its polarity. This, after a modest reduction in amplitude (due to either dispersion or damping), results in a reflected wave with a large negative pressure that now exceeds the cavitation threshold upon focusing near the droplet's center on the return pass [Fig. 3(b)]. After cavitation, the pressure wave continues to evolve and reflects to propagate toward the droplet center once again. However, it now meets a cavitation bubble. Provided that the size of the bubble after $\Delta t^* > 1$ is on the order of that of the pressure wave, it reflects off of it, effectively trapping the wave on the left-hand side between the droplet surface and cavitation bubble [see Figs. 3(c) and 3(d)].

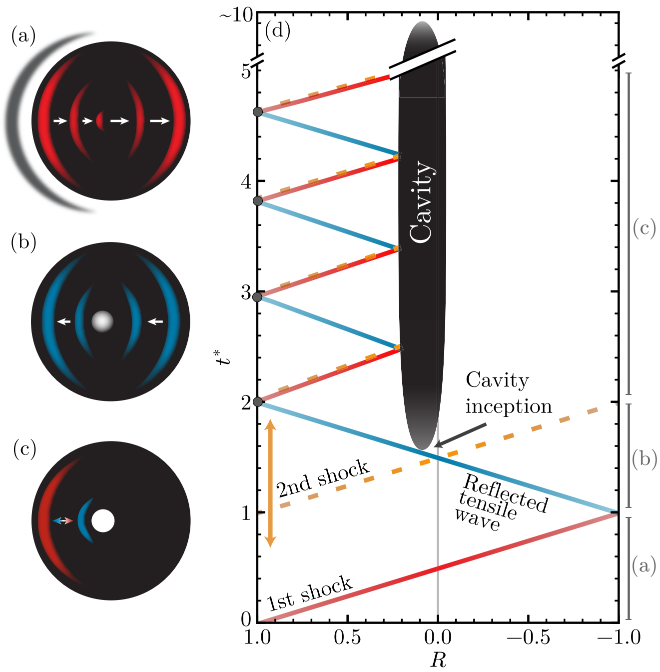

FIG. 3. (a)–(c) Illustrations of the three stages of the proposed model (see main text). (a) The first shock traverses the drop. (b) The shock reflects off the free surface on the right, inverting polarity, and traverses the droplet toward the left. As it focuses at the droplet center, it creates a cavitation bubble (not to scale) that can be made to collapse with a second shock. (c) After bubble formation, the first shock becomes trapped between the droplet's left surface and the cavitation bubble. Note that, although all shocks are in reality bipolar, shocks with a predominantly positive (negative) pressure amplitude are here depicted in red (blue) color only. (d) Schematic space-time diagram of shock propagation and cavity dynamics. The three regimes corresponding to illustrations [panels (a)–(c)] are indicated on the right.

The second pressure wave, induced by the second laser pulse [Fig. 3(c)], traverses the liquid, also to focus on the droplet center. This second pressure wave, for times $t > D_0/c$, will encounter the cavitation bubble that collapses under the action of this pressure wave. If the excitation of this second pressure wave exactly coincides with a reflection of the first wave [Fig. 3(d)], constructive interference leads to an increased pressure on the interface of the cavitation bubble, and an increased jet velocity. Small differences in timing lead to constructive and destructive interferences. The width of the individual sharp (constructive or negative) interferences is approximately $0.1t^*$ (~1 ns) at full width at half maximum [see inset in Fig. 2(d)] and does not significantly increase with delay time (indicating negligible further dispersion); the value is in line with expectations from Ref. [26] predicting a pressure wave with an approximate $0.1R_0/c \approx 1$ ns width.

No jetting is observed up to $t^* = 2$ for the nominal-energy cases, consistent with the fact that the cavitation bubble is created on the second pass of the wave in tandem with finite onset dynamics in the formation of the cavitation bubble. For the case of the twofold increase in pulse energy, the noninterference jetting starts slightly after $t^* = 1$ [cf. Fig. 2(d)], which may also be explained by cavitation after the first reflection [cf. Fig. 3(d)]. It should be clear that our experimental conditions were intentionally chosen to lie at the very threshold of jetting, and the significant 2× change in pulse energy for this outlier case, may lead to significant changes in the dynamics, such as the formation of a cavitation bubble that is larger, facilitating earlier puncturing of the droplet surface by a jet following bubble collapse.

From the decaying peak amplitudes, we find a $1/e$ decay time on the order of 40 ns, a value that appears to be independent of the pulse energy. The decay time of the baseline, however, is much longer and is dependent on pulse energy, consistent with the much longer timescale of the bubble dynamics.

V. BUBBLE DYNAMICS

For a noncavitated droplet, constructive interference would occur at $t^* = n$, assuming that the pressure waves propagate at the speed of sound c. However, from Fig. 2(d) it is clear that the peaks are shifted with respect to the dimensionless acoustic propagation time t^* and that they start from $n = 2$. The slight shift in the start of the interferences at $n = 2$ can be explained by an increase in the pressure-wave propagation velocity: It is due to the *round-trip* velocity being larger than c. For simplicity, we assume that a supersonic wave velocity only applies to the first $2D_0$ propagation, and take $c_s = c$ after $n = 2$. The measured offset yields a $c_s = 1.06c$ shock speed, a number that is consistent with the asymptotic value $1.07(2)c$ from Ref. [27] for large droplets or, equivalently, low pulse energies (recall the ratio E/R_0^3 [26]). The round-trip velocity is effectively the average of the velocities of the positive and negative waves. We also observe in Fig. 2(d) that all peaks for $n > 2$ are visibly shifted from $t^* = n$, which cannot be explained from any increase in shock-wave velocities alone. Instead, the shifts can be readily interpreted in terms of a reduction in path length due to the presence of a bubble.

The bubble dynamics are governed by the inviscid Rayleigh-Plesset equation (see, e.g., Refs. [46,47] or the more recent Refs. [1,48]) here adapted to the current special case of the pressure being dominated by the Laplace pressure, given the near-zero pressure in the vacuum chamber,

$$R(t)\ddot{R}(t) + \frac{3}{2}\dot{R}(t)^2 + \frac{2\sigma}{\rho R(t)} = 0, \qquad (1)$$

and in the limit of $R/R_0 \ll 1$ (the finite radius of the droplet R_0 here thus marginally impacts the bubble's dynamics [1]), and neglecting the vapor pressure inside the bubble in the expanded phase relevant here. R is the bubble radius and $\dot{R}$, $\ddot{R}$ are its time derivatives. This modified equation yields symmetric bubble growth and collapse, with a duration $t_s \approx \sqrt{3\rho R_M^3/\sigma}$, where R_M is the maximum bubble radius.

Figure 4 shows the positions of the various interference peaks from Fig. 2 as a function of n. The diagonal dashed line depicts the bubble-free expectation $t^* = n$, again underlining the fact that the peaks occur earlier than expected. A linear fit $y = ax + b$ describes the data well ($R^2 > 0.999$). From the fit, we can infer a path-length reduction $d = 1 - a = 0.200(4)D_0$ and reproduce the aforementioned supersonic wave velocity $c_s = 2/(2a + b) = 1.06(1)c$. Keeping the wave velocity constant at an upper limit of $1.06c$ instead, yields a

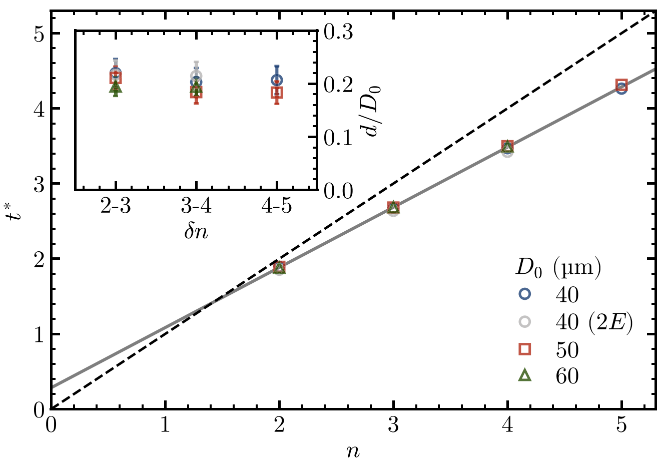

FIG. 4. Nondimensional peak position t^* as a function of peak number n for all the three studied droplet diameters. The dashed black line following $t^* = n$ is plotted as a visual guide. The gray solid line presents the results of a linear fit to the data. The inset shows the nondimensionalized change in path length d/D_0 for the interference peak spacings δn.

still constant, smaller path-length reduction of $d = 1 - a = 0.155(3)D_0$.

The path-length reduction can similarly be computed from the time differences between the constructive interference peaks $d = D_0 - c(t_n - t_{n-1})$, as shown in the inset in Fig. 4. The constancy of d/D_0, and in fact the overall dynamics (cf. Fig. 2), over droplet size is explained from our experimental conditions, where we keep E/R_0^3 constant following Grigoryev *et al.* [26], which enables a self-similar scaling of the dynamics to arbitrary droplet size. As emphasized by the inset of Fig. 4, the path-length reduction introduced by the presence of the bubble is approximately constant within the measured range ($n = 2 - 5$). This observation rules out the possibility of a centrally located bubble with a large diameter of $0.2D_0$, which would explain the path-length reduction, but would require an approximately microsecond period to reach its maximum size, far too long to be consistent with the observed constancy of d/D_0. Instead, the constant $d = 0.2D_0$ path-length reduction is straightforwardly explained by a slight offset of a smaller cavitation bubble from the droplet center, as may be expected from an imperfect shock focusing from a spherical shape and at large angles, in line with prior simulations [26].

From the baseline jetting velocity in Fig. 2, we infer a value for the bubble expansion and collapse time of $2t_s$ ranging from ~100 to 150 ns, which is consistent with a bubble of maximum diameter ranging from ~0.8 to 1.1 μm. Due to the fast dynamics involved, the bubble would already grow to >70% of its maximum size before $t^* = 2$, which supports the hypothesis that the bubble is then large enough to significantly reflect the shock wave (being on the order of the shock focal size). Note that an ~1-μm-sized bubble would indicate a 10^{-5}-level increase of the droplet's outer surface, far below the measurement accuracy. Furthermore, the fractional change in its small diameter (compared to its $0.2D_0$ offset) underpins the absence of any obvious temporal dynamic between $n = 2$ and 5 in the inset of Fig. 4.

VI. CONCLUSION

We presented observations pertaining to the interference of two subsequent laser-induced shock waves in a droplet, and to the creation of an ~100 m/s microjet through their joint action. The observed interference pattern is explained in terms of the inception of an offset, micrometer-sized cavitation bubble and the acoustic interference of pressure waves trapped between this cavity and the laser-facing free surface of the droplet. All extracted parameters, such as shock velocity, bubble size and dynamics, and interference width, are in good agreement with expectations. This laser-droplet system presents a unique, text-book-clear case for the study of acoustics and cavitation, with the spherical system focusing shocks with long coherence times. Future work may focus on using inspection of the interior of the droplet, e.g., using pulsed x-rays, to gain further direct insights on the shock and cavity dynamics.

ACKNOWLEDGMENTS

This work was conducted at the Advanced Research Center for Nanolithography (ARCNL), a public-private partnership between the University of Amsterdam (UvA), Vrije Universiteit Amsterdam (VU), Rijksuniversiteit Groningen (UG), the Dutch Research Council (NWO), and the semiconductor equipment manufacturer ASML. We thank Hugo Franca and Michel Versluis for useful discussions. The work of G.L. was supported by ERC Grant Super-FALCON, No. 101076844, funded by the European Union. Views and opinions expressed are those of the author(s) only and do not necessarily reflect those of the European Union or the European Research Council Executive Agency. Neither the European Union nor the granting authority can be held responsible for them.

DATA AVAILABILITY

The data that support the findings of this article are not publicly available because of legal restrictions preventing unrestricted public distribution. The data are available from the authors upon reasonable request.

[1] D. Obreschkow, P. Kobel, N. Dorsaz, A. De Bosset, C. Nicollier, and M. Farhat, Cavitation bubble dynamics inside liquid drops in microgravity, Phys. Rev. Lett. **97**, 094502 (2006).

[2] E. Zwaan, S. Le Gac, K. Tsuji, and C.-D. Ohl, Controlled cavitation in microfluidic systems, Phys. Rev. Lett. **98**, 254501 (2007).

[3] C. A. Stan *et al.*, Liquid explosions induced by x-ray laser pulses, Nat. Phys. **12**, 966 (2016).
[4] J. M. Rosselló, H. Reese, K. A. Raman, and C.-D. Ohl, Bubble nucleation and jetting inside a millimetric droplet, J. Fluid Mech. **968**, A19 (2023).
[5] S. T. Thoroddsen, K. Takehara, T. G. Etoh, and C.-D. Ohl, Spray and microjets produced by focusing a laser pulse into a hemispherical drop, Phys. Fluids **21**, 112101 (2009).
[6] D. Obreschkow, M. Tinguely, N. Dorsaz, P. Kobel, A. De Bosset, and M. Farhat, Universal scaling law for jets of collapsing bubbles, Phys. Rev. Lett. **107**, 204501 (2011).
[7] H. Reese, C.-D. Ohl, and J. M. Rosselló, Cavitation and jetting from shock wave refocusing near convex liquid surfaces, Int. J. Multiphase Flow **175**, 104822 (2024).
[8] C. A. Stan, P. R. Willmott, H. A. Stone, J. E. Koglin, M. Liang, A. L. Aquila, J. S. Robinson, K. L. Gumerlock, G. Blaj, R. G. Sierra, S. Boutet, S. A. Guillet, R. H. Curtis, S. L. Vetter, H. Loos, J. L. Turner, and F. J. Decker, Negative pressures and spallation in water drops subjected to nanosecond shock waves, J. Phys. Chem. Lett. **7**, 2055 (2016).
[9] S. R. G. Avila and C.-D. Ohl, Fragmentation of acoustically levitating droplets by laser-induced cavitation bubbles, J. Fluid Mech. **805**, 551 (2016).
[10] M. S. Krivokorytov, Q. Zeng, B. V. Lakatosh, A. Y. Vinokhodov, Y. V. Sidelnikov, V. O. Kompanets, V. M. Krivtsun, K. N. Koshelev, C.-D. Ohl, and V. V. Medvedev, Shaping and controlled fragmentation of liquid metal droplets through cavitation, Sci. Rep. **8**, 597 (2018).
[11] S. Y. Grigoryev, B. V. Lakatosh, P. M. Solyankin, M. S. Krivokorytov, V. V. Zhakhovsky, S. A. Dyachkov, C.-D. Ohl, A. P. Shkurinov, and V. V. Medvedev, Jet effusion from a metal droplet irradiated by a polarized ultrashort laser pulse, Phys. Rev. Appl. **18**, 024072 (2022).
[12] A. Vogel, W. Lauterborn, and R. Timm, Optical and acoustic investigations of the dynamics of laser-produced cavitation bubbles near a solid boundary, J. Fluid Mech. **206**, 299 (1989).
[13] A. Philipp and W. Lauterborn, Cavitation erosion by single laser-produced bubbles, J. Fluid Mech. **361**, 75 (1998).
[14] D. Obreschkow, N. Dorsaz, P. Kobel, A. De Bosset, M. Tinguely, J. Field, and M. Farhat, Confined shocks inside isolated liquid volumes: A new path of erosion? Phys. Fluids **23**, 101702 (2011).
[15] S. R. Gonzalez-Avila, F. Denner, and C.-D. Ohl, The acoustic pressure generated by the cavitation bubble expansion and collapse near a rigid wall, Phys. Fluids **33**, 032118 (2021).
[16] C.-D. Ohl and R. Ikink, Shock-wave-induced jetting of micron-size bubbles, Phys. Rev. Lett. **90**, 214502 (2003).
[17] P. Prentice, A. Cuschieri, K. Dholakia, M. Prausnitz, and P. Campbell, Membrane disruption by optically controlled microbubble cavitation, Nat. Phys. **1**, 107 (2005).
[18] S. Mitragotri, Current status and future prospects of needle-free liquid jet injectors, Nat. Rev. Drug Discov. **5**, 543 (2006).
[19] J. Schoppink and D. F. Rivas, Jet injectors: Perspectives for small volume delivery with lasers, Adv. Drug Delivery Rev. **182**, 114109 (2022).
[20] J. M. Rosselló and C.-D. Ohl, Bullet jet as a tool for soft matter piercing and needle-free liquid injection, Biomed. Opt. Express **13**, 5202 (2022).
[21] M. M. Basko, M. S. Krivokorytov, A. Yu Vinokhodov, Y. V. Sidelnikov, V. M. Krivtsun, V. V. Medvedev, D. A. Kim, V. O. Kompanets, A. A. Lash, K. N. Koshelev, and A. Y. Vinokhodov, Fragmentation dynamics of liquid-metal droplets under ultrashort laser pulses, Laser Phys. Lett. **14**, 036001 (2017).
[22] S. A. Reijers, J. H. Snoeijer, and H. Gelderblom, Droplet deformation by short laser-induced pressure pulses, J. Fluid Mech. **828**, 374 (2017).
[23] M. S. Krivokorytov, A. Yu Vinokhodov, Y. V. Sidelnikov, V. M. Krivtsun, V. O. Kompanets, A. A. Lash, K. N. Koshelev, and V. V. Medvedev, Cavitation and spallation in liquid metal droplets produced by subpicosecond pulsed laser radiation, Phys. Rev. E **95**, 031101(R) (2017).
[24] A. S. Stodolna, T. d. F. Pinto, F. Ali, A. Bayerle, D. Kurilovich, J. Mathijssen, R. Hoekstra, O. O. Versolato, K. S. E. Eikema, and S. Witte, Controlling ion kinetic energy distributions in laser produced plasma sources by means of a picosecond pulse pair, J. Appl. Phys. **124**, 053303 (2018).
[25] D. Kurilovich, T. F. Pinto, F. Torretti, R. Schupp, J. Scheers, A. S. Stodolna, H. Gelderblom, K. S. E. Eikema, S. Witte, W. Ubachs, R. Hoekstra, and O. O. Versolato, Expansion dynamics after laser-induced cavitation in liquid tin microdroplets, Phys. Rev. Appl. **10**, 054005 (2018).
[26] S. Y. Grigoryev, B. V. Lakatosh, M. S. Krivokorytov, V. V. Zhakhovsky, S. A. Dyachkov, D. K. Ilnitsky, K. P. Migdal, N. A. Inogamov, A. Y. Vinokhodov, V. O. Kompanets, Y. V. Sidelnikov, V. M. Krivtsun, K. N. Koshelev, and V. V. Medvedev, Expansion and fragmentation of liquid metal droplet by a short laser pulse, Phys. Rev. Appl. **10**, 064009 (2018).
[27] R. A. Meijer, R. Schupp, J. Sheil, M. M. Basko, K. S. E. Eikema, O. O. Versolato, and S. Witte, Spall-velocity reduction in double-pulse impact on tin microdroplets, Phys. Rev. Appl. **16**, 024026 (2021).
[28] D. Kurilovich, A. L. Klein, F. Torretti, A. Lassise, R. Hoekstra, W. Ubachs, H. Gelderblom, and O. O. Versolato, Plasma propulsion of a metallic microdroplet and its deformation upon laser impact, Phys. Rev. Appl. **6**, 014018 (2016).
[29] R. A. Meijer, Tailored laser-droplet interaction, Ph.D. thesis, Vrije Universiteit Amsterdam, 2021.
[30] R. A. Meijer, A. S. Stodolna, K. S. E. Eikema, and S. Witte, High-energy Nd:YAG laser system with arbitrary subnanosecond pulse shaping capability, Opt. Lett. **42**, 2758 (2017).
[31] T. D. F. Pinto, J. Mathijssen, R. A. Meijer, H. Zhang, A. Bayerle, D. Kurilovich, O. O. Versolato, K. S. E. Eikema, and S. Witte, Cylindrically and non-cylindrically symmetric expansion dynamics of tin microdroplets after ultrashort laser pulse impact, Appl. Phys. A **127**, 93 (2021).
[32] J. Hernandez-Rueda, B. Liu, D. J. Hemminga, Y. Mostafa, R. A. Meijer, D. Kurilovich, M. Basko, H. Gelderblom, J. Sheil, and O. O. Versolato, Early-time hydrodynamic response of a tin droplet driven by laser-produced plasma, Phys. Rev. Res. **4**, 013142 (2022).
[33] R. A. Meijer, D. Kurilovich, B. Liu, Z. Mazzotta, J. Hernandez-Rueda, O. O. Versolato, and S. Witte, Nanosecond laser ablation threshold of liquid tin microdroplets, Appl. Phys. A **128**, 570 (2022).
[34] D. Hudgins, Advanced irradiation schemes for target shaping in droplet-based laser-produced plasma light sources, Ph.D. thesis, ETH, Zürich, 2019.

[35] A. Antkowiak, N. Bremond, S. Le Dizès, and E. Villermaux, Short-term dynamics of a density interface following an impact, J. Fluid Mech. **577**, 241 (2007).

[36] Y. Tagawa, N. Oudalov, C. W. Visser, I. R. Peters, D. van der Meer, C. Sun, A. Prosperetti, and D. Lohse, Highly focused supersonic microjets, Phys. Rev. X **2**, 031002 (2012).

[37] G. Birkhoff, D. P. MacDougall, E. M. Pugh, and G. Taylor, Explosives with lined cavities, J. Appl. Phys. **19**, 563 (1948).

[38] T. de Rességuier, E. Lescoute, A. Sollier, G. Prudhomme, and P. Mercier, Microjetting from grooved surfaces in metallic samples subjected to laser driven shocks, J. Appl. Phys. **115**, 043525 (2014).

[39] N. A. Hawker and Y. Ventikos, Interaction of a strong shockwave with a gas bubble in a liquid medium: A numerical study, J. Fluid Mech. **701**, 59 (2012).

[40] S. Sembian, M. Liverts, N. Tillmark, and N. Apazidis, Plane shock wave interaction with a cylindrical water column, Phys. Fluids **28**, 056102 (2016).

[41] Y. Liang, Y. Jiang, C. Y. Wen, and Y. Liu, Interaction of a planar shock wave and a water droplet embedded with a vapour cavity, J. Fluid Mech. **885**, R6 (2020).

[42] K. Schmidmayer and L. Biasiori-Poulanges, Geometry effects on the droplet shock-induced cavitation, Phys. Fluids **35**, 063315 (2023).

[43] G. N. Sankin, W. N. Simmons, S. L. Zhu, and P. Zhong, Shock wave interaction with laser-generated single bubbles, Phys. Rev. Lett. **95**, 034501 (2005).

[44] P. W. Humrickhouse, An equation of state and compendium of thermophysical properties of liquid tin, a prospective plasma-facing material, IEEE Trans. Plasma Sci. **47**, 3374 (2019).

[45] T. Paula, S. Adami, and N. A. Adams, Analysis of the early stages of liquid-water-drop explosion by numerical simulation, Phys. Rev. Fluids **4**, 044003 (2019).

[46] L. Rayleigh, VIII, On the pressure developed in a liquid during the collapse of a spherical cavity, London, Edinburgh, Dublin Philos. Mag. J. Sci. **34**, 94 (1917).

[47] A. Prosperetti, A generalization of the Rayleigh-Plesset equation of bubble dynamics, Phys. Fluids **25**, 409 (1982).

[48] R. A. Van Gorder, Dynamics of the Rayleigh–Plesset equation modelling a gas-filled bubble immersed in an incompressible fluid, J. Fluid Mech. **807**, 478 (2016).